Thermal-disrupting interface mitigates intercellular cohesion loss for accurate topical antibacterial therapy

Hu, Benhui; Berkey, Christopher; Feliciano, Timothy; Chen, Xiaohong; Li, Zhuyun; Chen, Chao; Amini, Shahrouz; Nai, Mui Hoon; Lei, Qun-Li; Ni, Ran; Wang, Juan; Leow, Wan Ru; Pan, Shaowu; Li, Yong-Qiang; Cai, Pingqiang; Miserez, Ali; Li, Shuzhou; Lim, Chwee Teck; Wu, Yun-Long; ...Chen, Xiaodong

2020

Hu, B., Berkey, C., Feliciano, T., Chen, X., Li, Z., Chen, C., Amini, S., Nai, M. H., Lei, Q., Ni, R., Wang, J., Leow, W. R., Pan, S., Li, Y., Cai, P., Miserez, A., Li, S., Lim, C. T., Wu, Y., ...Chen, X. (2020). Thermal-disrupting interface mitigates intercellular cohesion loss for accurate topical antibacterial therapy. Advanced Materials, 32(12), e1907030-. https://dx.doi.org/10.1002/adma.201907030

DOI: 10.1002/((please add manuscript number))
Article type: Communication

Thermal-disrupting interface mitigates intercellular cohesion loss for accurate topical antibacterial therapy

Benhui Hu, Christopher Berkey, Timothy Feliciano, Xiaohong Chen, Zhuyun Li, Chao Chen, Shahrouz Amini, Mui Hoon Nai, Qun-Li Lei, Ran Ni, Juan Wang, Wan Ru Leow, Shaowu Pan, Yong-Qiang Li, Pingqiang Cai, Ali Miserez, Shuzhou Li, Chwee Teck Lim, Yun-Long Wu,* Teri W. Odom,* Reinhold H. Dauskardt* and Xiaodong Chen**

Prof. B. Hu
Key Laboratory of Clinical and Medical Engineering, School of Biomedical Engineering and Informatics, Nanjing Medical University
Nanjing 211166, P.R. China

Prof. B. Hu, Dr. Z. Li, Dr. C. Chen, Dr. S. Amini, Dr. J. Wang, Dr. W. Leow, Dr. S. Pan, Dr. Y. Li, Dr. P. Cai, Prof. A. Miserez, Prof. S. Li, Prof. X. Chen
Innovative Centre for Flexible Devices (iFLEX), School of Materials Science and Engineering, Nanyang Technological University, 50 Nanyang Avenue, Singapore 639798, E-mail: chenxd@ntu.edu.sg

Dr. C. Berkey, Prof. R. Dauskardt
Department of Materials Science and Engineering, Stanford University, Stanford, CA 94305, E-mail: dauskardt@stanford.edu

Mr. T. Feliciano, Prof. T. Odom
Department of Materials Science and Engineering and Department of Chemistry, Northwestern University, Evanston, Illinois 60208, United States, E-mail: todom@northwestern.edu

Ms. X. Chen, Prof. Y. Wu
Fujian Provincial Key Laboratory of Innovative Drug Target Research and State Key Laboratory of Cellular Stress Biology, School of Pharmaceutical Sciences, Xiamen University, Xiamen, Fujian, 361102, P. R. China, E-mail: wuyl@xmu.edu.cn

Dr. M. Nai, Prof. C. Lim
Department of Biomedical Engineering, Mechanobiology Institute, Institute for Health Innovation and Technology (iHealthtech) National University of Singapore, 9 Engineering Drive 1, Singapore 117576, E-mail: ctlim@nus.edu.sg

Dr. Q. Lei, Prof. R. Ni

School of Chemical and Biomedical Engineering, Nanyang Technological University, 62 Nanyang Drive, 637459, Singapore;

Keywords: Biointerface, intercellular cohesion, thermal management, antibacterial therapy, wound healing

Abstract

Bacterial infections remain a leading threat to global health because of the misuse of antibiotics and the rise in drug resistant pathogens. Although several strategies such as photothermal therapy and magneto‐thermal therapy can suppress bacterial infections, excessive heat generated around the target sites often damage host cells and lengthen the healing time. Here, we report a localized thermal managing strategy, a thermal-disrupting interface induced mitigation (TRIM), to minimize intercellular cohesion loss for accurate antibacterial therapy. The TRIM dressing film is composed of alternative microscale arrangement of heat responsive hydrogel regions and mechanical support regions, which enables the surface microtopography to have a significant effect on disrupting bacterial colonization upon infrared irradiation. The regulation of the interfacial contact to the attached skin confines the produced heat and minimize the risk of skin damage and function loss during thermoablation. Quantitative mechanobiology studies demonstrate the TRIM dressing film with a critical dimension for surface feature plays a critical role in maintaining intercellular cohesion of epidermis during photothermal therapy. Finally, endowing wound dressing with TRIM effect via *in vivo* studies in *S. aureus* infected mice demonstrates a promising strategy for mitigating the side effect of photothermal therapy against a wide spectrum of bacterial infections, promoting future biointerface design for antibacterial therapy.

Introduction

Skin is the largest organ of human body and provides a vast interface for interactions with external environments,[1] while concomitantly containing symbiotic commensal microbiota.[2] Maintaining the skin's barrier against external harm under healthy conditions not only relies on the keratinized skin cells and skin immune system but also on the resident microbes from skin microbiota.[3] Imbalance of the skin microbiota due to either skin damage or assault of pathogens could initiate skin disorders and also infected wounds.[4] Particularly, improper or belated treatment would allow the invading and colonizing of pathogens, thereby leading to the failure of healing mechanism and even threatening the life of patients.[5] To prevent the pathogens impeding wound healing, substantial efforts have been made to develop dressing materials incorporating antibacterial drugs (antibiotics) and tissue regenerative agents.[6] Nevertheless, worldwide misuse of these drugs is causing pathogens to become drug-resistant, making infections harder to treat,[7] and also increasing the risk of depleting resident microbiota.[8]

Thermoablation has emerged as an effective treatment modality against most common pathogens even after drug-resistance has been developed.[9] However, conventional thermoablative approaches, which produce macroscopic heat sources for thermal destruction, can threaten the surrounding normal tissues and form severe systemic side effects.[10] To downscale the heat sources and reduce injuries, photo-absorbing nanocomposites have been used to allow ablations to be carried out photothermally.[11] To date, most accurate photothermal therapies are accomplished by

direct administration of nanocomposite to target regions of interest *in vivo*, yet residual nanocomposites can cause post-therapeutic toxicity.[12] To circumvent residual toxicity, nanocomposites have been encapsulated in matrices as dressing materials for treating skin disorders.[13] However, the undesirable heat distribution during photothermal therapy could mechanically harm the intercellular cohesion energy of skin tissue and inhibit the restoration of barrier function.[14] Therefore, thermal management and heat transfer at the biointerface between dressing matrix and cutaneous tissue remains a challenge.

Here, we report a new localized thermal managing strategy, the so called thermal-disrupting interface induced mitigation (TRIM), to reduce cohesion loss of epidermis tissue during thermoablation of microbes, thereby functioning as an extracellular biointerface for precise topical antibacterial therapy. The TRIM film is composed of heat responsive hydrogel regions and mechanical support elastomer regions. The alternative microscale arrangement of these two regions enables the surface microtopography to have a significant effect on disrupting bacterial colonization and dispersing individual bacteria sensitive to heat. More importantly, the thermal responsive regions can shrink upon infrared-light irradiation, enabling the regulation of the interfacial contact to the attached skin, thereby confining the produced heat and minimizing the risk of skin damage and function loss during thermoablation (Figure 1a). In particular, a quantitative correlation between the interfacial contact and thermal effect on reducing intercellular cohesion energy within the epidermis is established. Our results demonstrate that the film with a critical dimension for surface feature, which is

larger than single bacterial cell and smaller than single mammalian cell, would smartly reduce the interfacial contact and significantly maintain the intercellular cohesion of the stratum corneum (SC), the critical outermost layer of the epidermis, while effectively eliminating surrounding bacteria under infrared-light irradiation. Although thin, the SC elastic modulus is up to three orders of magnitude larger than that of deeper skin layers, giving it dominance over local stresses and perception within the skin.[15] Endowing wound dressing with TRIM effect demonstrates a promising strategy for mitigating the side effect of photothermal therapy against a wide spectrum of bacterial infections, promoting next-generation biointerface design for accurate antibacterial therapy.

Results and Discussion

Surface microtopography improves photothermal decontamination. To effectively cure the cutaneous infection by bacteria, the dressing film is enabled to inhibit the aggregation of bacteria and biofilm formation.[16] Inspired by the shark skin, which deters marine organisms from attaching and growth,[17] we decorated microtopography by imparting adhesion resistance to the biointerface to prevent bacteria aggregating (Figure 1b left). By integrating a thermal-responsive material on the micro-featured surface, we created a flat surface exhibiting more contact with cutaneous tissue and higher chance capturing bacteria. During thermoablation, the heat induced response would reproduce the corrugated microtopography. This adaptivity ensures the disruption of biofilm and promotes elimination of captured bacteria (Figure 1b right),

because reducing the possibility of biofilm formation can lower the tolerance of pathogen to therapeutic agents. In our case, the required irradiation dosage to eliminate pathogens is accordingly reduced, which in turn mitigate the unexpected thermoablative damage on healthy skin. Proper selection for the dimension of topography based on the cut-off size between bacteria (normally 0.2-2.0 μm in diameter) and host cells (normally larger than 5 μm) can lead to species-specific spatial confinement, where bacteria demonstrate preferential attachment sites located in the depressed regions while host cells can only attach to raised regions[18]. To address the dimension-dependent effect of topographic features on disrupting biofilm formation, we prepared polydimethylsiloxane (PDMS)-based flexible substrates with six different feature sizes (2 μm, 3 μm, 5 μm, 7 μm, 10 μm and 20 μm for gap width) and studied the growth of *Staphylococcus aureus* (*S. aureus*) on each. When allowed to grow on surfaces with 2-μm and 3-μm features, *S. aureus* attached preferentially in the gaps between features (Figure 1c). On surfaces with larger features (5 μm and above), *S. aureus* formed aggregates. These results show that larger surface features facilitated bacterial colonization and subsequent biofilm formation. This size-dependent aggregation of *S. aureus* is further shown quantitatively by plotting contamination ratio (*i.e.* ratio between contaminated area to the substrate area) as a function of surface feature size (Figure 1d). Because bacteria within biofilms are more resistant to antimicrobial agents, killing them become more difficult. As illustrated in Figure 1d, the decontamination ratio (*i.e.* ratio between killed bacteria number and total bacteria number) decreased from ~95% to ~33% when the feature size increases from 2 μm to

20 μm. It is worth noting that although substrates with 3-μm and 2-μm features showed nearly equal killing efficiency, the 3-μm substrate showed greater bacterial capture and mechanical stability (smaller features are more easily collapsed).[19] Thus, we choose 3 μm as the optimal feature size.

***In vitro* antibacterial performance of thermal-disrupting interface.** To produce thermal-disrupting interface for photothermal therapy, we locally incorporated gold nanostars (AuNS),[20] which convert photon energy into highly concentrated heating based on the plasmonics-enhanced photothermal property. Because these nanostars have extended branches (~14 nm), they display a 300 nm red-shifted absorbance peak maximum relative to spherical gold nanoparticles (Figure S1a, b). To distribute the AuNS in the depressed regions of the biomimetic PDMS surface, we used poly(N-isopropylacrylamide) (pNIPAM) hydrogel to immobilize the AuNS.[21] Because pNIPAM has a sensitive thermal response,[22] it shrinks towards the surface features upon infrared irradiation. This ensures the AuNS, which produce extreme and localized heat upon irradiation, are at a safe distance from the host cells. Furthermore, the thin pNIPAM coating (thickness roughly equal to the height of PDMS surface feature) helps maintain moisture and rehydrate the surface, allowing the integrated bilayer to conform to the skin and sustainably contact bacteria at the infection site.

To enable the adaptivity of the interface, droplet of pNIPAM precursor mixed with AuNS was delivered into the microvalleys between the microridges of PDMS by capillary force (Figure S2). After polymerization, most of the AuNS were found within the depressed region of the PDMS substrate where planktonic bacteria preferentially

attach to (Figure 2a). This spatial distribution of the AuNS photothermal agents allows bacteria to be photothermally destroyed without damaging the host cells. UV-vis absorption spectroscopy showed that the absorbance of the PDMS-pNIPAM bilayer films in the visible and near-infrared (NIR) regions depended on the size of the surface features (Figure 2b). Because of the geometrically enhanced optical path length, films with smaller features exhibited higher absorbance and thus, higher energy conversion efficiency that those with larger features. This is further confirmed by Finite-Difference Time-Domain (FDTD) simulations (Figure 2c). At AuNS concentration of 0.2 nM, the global average temperature of the film was maintained below 60 °C (~58 °C) when irradiated by NIR at a power density of 70 mW/cm^2 (Figure 2d). Cyclic irradiation shows the response of our films is rapid (surface temperature is increased to over 50 °C within a minute upon NIR irradiation) and reversible (Figure S3).

We next studied the *in vitro* photothermal therapeutic efficacy of thermal-disrupting interface towards model gram-negative bacterium, *Escherichia coli* (*E. coli*) and *Pseudomonas aeruginosa* (*P. aeruginosa*), and the gram-positive bacterium, *S. aureus*.[23] Cultures of the three different bacteria were separately centrifuged and resuspended in PBS to be incubated on the PDMS-pNIPAM bilayer film with feature size of 3 μm (TRIM films) or flat films at a concentration of approximately 1×10^8 colony-forming units (CFU). After 30 min of NIR irradiation, survival curves of the three types of bacteria showed that TRIM films had better therapeutic efficacy than flat films (Figure 2e). This is consistent with the previous assertion that the adaptive microvalleys could concentrate AuNS, selectively trap and eliminate the preferentially

attached bacteria cells, whose tolerance to heat is also weakened in individual dispersion.

Topographically transformable properties of TRIM film. To evaluate the influence of temperature on the topography of our TRIM films, we characterized the surface topography of our films by atomic-force microscopy (AFM) and scanning electron microscopy (SEM) at two different temperatures (25 °C and 42 °C) (Figure 3a and Figure S4a-c). As shown in Figure 3b, the height difference between the microridges and microvalleys is less than 0.5 μm at temperatures lower than the lower critical solution temperature (LCST) of pNIPAM (32 °C), facilitating bacterial contact with depressed regions. In contrast, this height difference was enlarged to roughly 3 μm at temperatures above the LCST of pNIPAM. This thermo-responsive behavior enables the topography of the TRIM films to be transformed with temperature, offering a way to spatially confine bacteria to the depressed regions where the AuNS are concentrated while the host cells are distributed on the surrounding microridges. Simulation on the near field of infrared ray showed that the localized heat generation is more concentrated within gaps rather than elevated microridges (Figure S5), allowing bacteria in the gaps to be effectively destroyed photothermally while leaving host cells on the microridges unharmed.

Further, the height difference between the microridges and depressed gaps was maintained even when the TRIM films were stretched (Figure 3c), demonstrating the flexibility of the films. Nanoindentation studies further showed that TRIM films matched the mechanical compliance of human skin (with stiffness of 0.01 N/mm).[24]

Our measurements done in hydrated conditions revealed that the stiffness of TRIM film at 25 °C was 0.007 ± 0.001 N/mm while there was an increase to 0.011 ± 0.001 N/mm at 40 °C (Figure S6).

In addition, we used Madin-Darby canine kidney (MDCK) epithelial cells to study the selective cytotoxicity of the TRIM films. Cells were cultured on either TRIM or flat film and allowed to grow to ~80% confluency. For cytocompatibility studies, cells were exposed to NIR irradiation for 1 hour and subsequently co-stained with Calcine AM and propidium iodide (PI) to differentiate live cells (green) from dead cells (red). Confocal fluorescence microscopy imaging showed that MDCK cells were suspended above the depressed regions of the TRIM film (Figure 3d) and nearly all the cells survived after irradiation (Figure 3e inset), demonstrating that the space between epithelial sheets and AuNS-concentrated depressed regions can effectively prevent epithelial cell damage. In contrast, cells cultured on flat films demonstrated a mortality of around 30% (Figure 3e, f), further indicating that the heat killing effect works *via* an 'on-contact mechanism'.[25] In a positive control experiment where MDCK cells on TRIM films were irradiated with ultraviolet (UV) light (450 mW/cm^2, 40 mins), nearly 100% of the cells had died. Taken together, these results suggest that TRIM films with biomimetic microstructures results in a distribution of photothermal agents that effectively kills bacteria while protecting the survival of host cells (Figure 3g).

Rationale for mitigating the exposure-induced intercellular cohesion loss. To further demonstrate the biocompatibility and safety of our TRIM films for photothermal therapy, we investigated the effects of heat produced by NIR exposure on the

mechanical integrity of epidermis tissue. The SC, the outermost layer of the human epidermis and our body's main line of defense against external threat, was isolated and attached beneath films with different surface features. After NIR exposure with a certain dosage (70 mW/cm^2 by 30 mins) able to kill *S. aureus* determined from an *in vitro* study, the SC tissue was characterized by a double-cantilever beam (DCB) fracture mechanics method, in which the delamination energy (energy required for separating intercellular boundaries) was measured. This delamination energy directly characterizes the intercellular cohesion, which represents the mechanical integrity and thus, barrier function of the SC tissue. The critical load to propagate a crack in SC attached on a flat film was around 40% lower than on a TRIM film with a critical feature size of 3 μm (Figure 4a). Successive DCB measurements of the delamination energy through the thickness of the SC demonstrated that heat-induced cohesion loss is mostly concentrated on the superficial layers rather than the deeper layers, illustrating the cohesion energy is sensitive to the distance of the heat source (Figure 4b). To further elucidate the effect of biointerface topography on intercellular cohesion of the exposed SC, we varied the critical feature size to 7 μm, 20 μm and 60 μm. The DCB results show that larger feature size leads to lower intercellular cohesion (Figure 4b, inset). This suggests that the topography of TRIM films regulates heat transfer at the biointerface, which, in turn, affects the critical intercellular cohesion.

To prove the effect of topography on heat transfer through the biointerface between the films and SC, we developed a model to calculate the thermal resistance of each film with a compound thermal conducting layer.[26] The surface of our TRIM film is

composed of PDMS-based microridges and hydrogel-based microvalleys (Figure 4c, left). Upon heating, the responsive hydrogel would shrink and leave a headspace between the hydrogel and SC. Based on the organization, the thermal resistance of the microvalley (R_v) connects in parallel with the resistance of the microridge (R_r), while in the microvalley regions, the thermal hydrogel resistance (R_h) and the air resistance (R_a) are in series (Figure 4c, right and Figure 4d). When the width/depth ratio of the microvalley becomes larger (*e.g.* critical width of 20 μm and 60 μm, both with depth of 5 μm), the hydrogel roof can collapse and partially contact the SC. In this case, the effective thermal resistance (R_e) becomes (Figure 4e, f):

$$\frac{1}{R_e} = \frac{1}{R_{v'}} + \frac{1}{R_{f'}} + \frac{1}{R_r} = \frac{xA}{2}\frac{k_h k_a}{L_h k_a + L_a k_h} + \frac{(1-x)A}{2}\frac{k_h}{L_h} + \frac{A}{2}\frac{k_{pdms}}{L_r} \quad (1)$$

where L is the heat transfer distance (cm) within the film, k is the thermal conductivity (W/cm·K) and A is the effective cross-sectional area (cm^2) for heat transfer, while x is the ratio of unsagged width to the critical width. Based on the formulas, we found that a topography with a critical width of 3 μm would produce the highest thermal resistance through the biointerface. This strategy is similar to the use of surface texture to manage heat dissipation in microelectronics engineering.[27] Plotting out the cohesion energy loss (ΔG_c) with the reciprocal of thermal resistance demonstrates a logarithmic relationship (Figure 4g), which could be expressed as:

$$\Delta G_c \propto \ln \frac{1}{R_e A} \quad (2)$$

During irradiation, the TRIM films become apparently more rigid as the pNIPAM shrinks. This would prohibit the conformable attachments of film onto the rough skin and reduce the heat load reaching the biointerface and deeper epidermis (Figure S7a).

Mapping the temperature distribution further proves the role of microtopography in modulating thermal stress in SC (Figure S7b). In fact, the increased thermal resistance of dressing films with smaller critical topographical size results in an enlarged temperature gradient along the epidermic depth direction. This lowers the temperature at the biointerface and mitigates the cellular cohesion loss of the SC layer (Figure S7c). Therefore, this model confirms that rational topographical design can modulate thermal resistance of the film-skin biointerface by dissipating heat and reducing heat-induced mechanical damage in tissues.

***In vivo* antibacterial performance of TRIM films on a mouse model of *S. aureus* skin infection.** As a demonstration of the therapeutic efficacy of this approach, we performed the *in vivo* antibacterial performance of the TRIM films was assessed using a mouse model of *S. aureus* skin infection.[28] BALB/c female nude mice were shaved and inoculated subcutaneously with 100 μL of 1×10^9 live transformed *S. aureus* in sterile DPBS. When the abscess could be visualized at the infection site, the mice were randomly divided into six groups with each receiving a different treatment at the infection site: 1) TRIM films and 30 min of NIR irradiation daily; 2) flat films and the same irradiation dose as group 1; 3) commercial antibacterial hydrogel encapsulated with silver nanoparticles; 4) direct injection of AuNS at amounts comparable to group 3 and the same irradiation dose as group 1; 5) no treatment; and 6) NIR irradiation alone at the same dose as group 1 (Figure S8). The severity of *S. aureus* infection was characterized by the total radiant efficiency from the region of interest (ROI). Animals treated with TRIM films showed the most rapid decay in fluorescence intensity,

indicating the fastest loss of live *S. aureus* and thus, the best healing performance at the infection site (Figure 5a, b and Figure S9). Although the therapeutic efficacy of flat films (group 2) is lower than TRIM films (group 1), it remains better than the other four groups (Figure 5b). Treatments with either flat films or AuNS injection led to observable skin damage. As shown in Figure S10, the infection progressed and resulted in significant ulcerations in group 3 and 4, suggesting that without the controlled spatial distribution of photothermal agents, global overheating can harm host cells. In positive control experiments (group 5 and 6), despite neutrophil clearance of *S. aureus* infection,[29] abscesses remained after 6 days with increasing dermal edema (Figure S10. These results are consistent with the *in vitro* studies, further demonstrating that the biomimetic microtopography is crucial for therapeutic efficacy.

Histology by Hematoxylin/Eosin (H&E) staining was further performed to investigate the inflammatory response of surrounding tissue within the infected sites. As shown in Figure 5c, mice treated with TRIM films (group 1) demonstrated abundant regenerated granulation tissue within normal epithelial structures, proving its potential as an effective local dressing against bacterial infection. However, in tissues from mice treated with flat films, necrosis and apparent inflammatory responses were found in both the epidermis and dermis, indicating the side effect of unconfined global heating (Figure 5d). Furthermore, in mice treated with silver-containing hydrogel, necrosis and inflammatory reaction remained even after 3 weeks of treatment (Figure 5e). In other groups (injection of AuNS, no treatment and bare IR irradiation), histological exam demonstrated extensive cell necrosis with neutrophil infiltration, leading to loose tissue

architecture with severe edema (Figure 5f, g and Figure S11). Overall, the minimal inflammation response seen in group 1 suggests that our TRIM film is effective at curing infection and promoting recovery.

Conclusion

In summary, we have developed a localized thermal managing strategy based on thermal-disrupting interface induced mitigation for accurate topical antibacterial therapy. Our TRIM film is made of PDMS with patterned microridges and microvalleys, and a layer of heat sensitive pNIPAM hydrogel used to immobilize AuNS for photothermal therapy. The 3-μm wide microridges and microvalleys on the PDMS film directed the attachment of bacterial cells to the microvalleys and host cells to the microridges. Upon irradiation with a modest intensity (70 mW/cm^2) of infrared irradiation, pNIPAM shrinks and localizes the AuNS in the microvalleys, concentrating the photothermal agents near the bacteria. This spatial distribution of AuNS keeps the heat at a safe distance from host cells and allows bacterial cells to be effectively killed photothermally while sparing host cells. Delamination measurements on the isolated human SC tissues further demonstrated the films with critical topographical features could significantly reduce intercellular cohesion loss during NIR irradiation, suggesting the contribution of topography on maintaining mechanical integrity and barrier function of skin for photothermal therapy. *In vivo* studies in *S. aureus* infected mice showed that our TRIM films were effective at eliminating infection and promoting wound healing.

Supporting Information

Supporting Information is available from the Wiley Online Library or from the author.

Acknowledgement. This work was financially supported by the NTU-Northwestern Institute for Nanomedicine and the National Research Foundation, Prime Minister's Office, Singapore, under the NRF Investigatorship (NRF-NRFI2017-07).

Author contributions. B.H., C.B., C.T.L., T.W.O., R.H.D. and X.D.C. designed research; B.H., C.B., T.F., X.C., Z.L., S.A., M.H.N., J.W., S.P., Y.Q.L., P.C. and Y.L.W. performed research; T.F. and S.A. contributed new reagents/analytic tools; B.H., C.C., S.A., Q.L.L., R.N., A.M. and S.L. analyzed data; C.T.L., T.W.O., R.H.D. and X.D.C. supervised the project; and B.H., W.R.L., C.B., C.T.L., T.W.O., R.H.D. and X.D.C. wrote the paper.

Conflict of Interest

The authors declare no conflict of interest.

Reference

[1] R. L. Gallo, *J. Invest. Dermatol.* **2017**, *137*, 1213.

[2] Y. Belkaid, J. A. Segre, *Science* **2014**, *346*, 954.

[3] E. A. Grice, J. A. Segre, *Nat. Rev. Microbiol.* **2011**, *9*, 244.

[4] Y. E. Chen, M. A. Fischbach, Y. Belkaid, *Nature* **2018**, *553*, 427.

[5] R. Peyraud, M. Mbengue, A. Barbacci, S. Raffaele, *Proc. Natl. Acad. Sci. U. S. A.* **2019**, *116*, 3193.

[6] a) K. Y. Zheng, M. I. Setyawati, T. P. Lim, D. T. Leong, J. P. Xie, *ACS Nano* **2016**, *10*, 7934; b) S. H. Cha, J. Hong, M. McGuffie, B. Yeom, J. S. VanEpps, N. A. Kotov, *ACS Nano* **2015**, *9*, 9097; c) L. L. Li, J. H. Xu, G. B. Qi, X. Z. Zhao, F. Q. Yu, H. Wang, *ACS Nano* **2014**, *8*, 4975; d) J. Zhou, D. Y. Yao, Z. Y. Qian, S. Hou, L. H. Li, A. T. A. Jenkins, Y. B. Fan, *Biomaterials* **2018**, *161*, 11; e) X. Zhao, B. L. Guo, H. Wu, Y. P. Liang, P. X. Ma, *Nat. Commun.* **2018**, *9*, 2784; f) Z. J. Fan, B. Liu, J. Q. Wang, S. Y. Zhang, Q. Q. Lin, P. W. Gong, L. M. Ma, S. R. Yang, *Adv. Funct. Mater.* **2014**, *24*, 3933; g) S. R. Modi, H. H. Lee, C. S. Spina, J. J. Collins, *Nature* **2013**, *499*, 219; h) P. A. Smith, M. F. T. Koehler, H. S. Girgis, D. H. Yan, Y. S. Chen, Y. Chen, J. J. Crawford, M. R. Durk, R. I. Higuchi, J. Kang, J. Murray, P. Paraselli, S. Park, W. Phung, J. G. Quinn, T. C. Roberts, L. Rouge, J. B. Schwarz, E. Skippington, J. Wai, M. Xu, Z. Y. Yu, H. Zhang, M. W. Tan, C. E. Heise, *Nature* **2018**, *561*, 189.

[7] a) J. M. A. Blair, M. A. Webber, A. J. Baylay, D. O. Ogbolu, L. J. V. Piddock, *Nat. Rev. Microbiol.* **2015**, *13*, 42; b) T. M. Gross, J. Lahiri, A. Golas, J. Luo, F. Verrier, J. L. Kurzejewski, D. E. Baker, J. Wang, P. F. Novak, M. J. Snyder, *Nat. Commun.* **2019**, *10*, 1979; c) X. Li, H. T. Bai, Y. C. Yang, J. Yoon, S. Wang, X. Zhang, *Adv. Mater.* **2019**, *31,* 1805092; d) Y. Si, Z. Zhang, W. R. Wu, Q. X. Fu, K. Huang, N. Nitin, B. Ding, G. Sun, *Sci. Adv.* **2018**, *4,* e5931.

[8] T. G. Sana, D. M. Monack, *Nature* **2016**, *534*, 624.

[9] K. F. Chu, D. E. Dupuy, *Nat. Rev. Cancer* **2014**, *14*, 199.

[10] a) K. Shinohara, *Int. J. Hyperther.* **2004**, *20*, 679; b) X. Q. Huang, S. H. Tang, X. L. Mu, Y. Dai, G. X. Chen, Z. Y. Zhou, F. X. Ruan, Z. L. Yang, N. F. Zheng, *Nat. Nanotechnol.* **2011**, *6*, 28.

[11] a) X. J. Zhu, W. Feng, J. Chang, Y. W. Tan, J. C. Li, M. Chen, Y. Sun, F. Y. Li, *Nat. Commun.* **2016**, *7*, 10437; b) Y. Yang, Y. Y. Deng, J. B. Huang, X. Fan, C. Cheng, C. X. Nie, L. Ma, W. F. Zhao, C. S. Zhao, *Adv. Funct. Mater.* **2019**, *29*, 1905540.

[12] a) V. P. Zharov, K. E. Mercer, E. N. Galitovskaya, M. S. Smeltzer, *Biophys. J.* **2006**, *90*, 619; b) N. Beyth, Y. Houri-Haddad, A. Domb, W. Khan, R. Hazan, *Evid-Based Compl. Alt.* **2015**, *2015*, 246012.

[13] a) J. A. Sanford, R. L. Gallo, *Semin. Immunol.* **2013**, *25*, 370; b) A. Narcisi, R. Favaro, A. Costanzo, *Nat. Biomed. Eng.* **2017**, *1,* 0068.

[14] a) S. J. Wang, X. Q. Ma, X. H. Hong, Y. X. Cheng, Y. Tian, S. Zhao, W. F. Liu, Y. X. Tang, R. Z. Zhao, L. Song, Z. G. Teng, G. M. Lu, *ACS Nano* **2018**, *12*, 662; b) M. F. Leyva-Mendivil, A. Page, N. W. Bressloff, G. Limbert, *J. Mech. Behav. Biomed. Mater.* **2015**, *49*, 197.

[15] K. S. Wu, W. W. van Osdol, R. H. Dauskardt, *Biomaterials* **2006**, *27*, 785.

[16] a) V. Narasimhan, R. H. Siddique, J. O. Lee, S. Kumar, B. Ndjamen, J. Du, N. Hong, D. Sretavan, H. Choo, *Nat. Nanotechnol.* **2018**, *13*, 512; b) A. B. Tesler, P. Kim, S. Kolle, C. Howell, O. Ahanotu, J. Aizenberg, *Nat. Commun.* **2015**, *6,* 8649.

[17] F. D. Arisoy, K. W. Kolewe, B. Homyak, I. S. Kurtz, J. D. Schiffman, J. J. Watkins, *ACS Appl. Mater. Inter.* **2018**, *10*, 20055.

[18] C. J. Long, J. A. Finlay, M. E. Callow, J. A. Callow, A. B. Brennan, *Biofouling* **2010**, *26*, 941.

[19] D. Chandra, S. Yang, *Accounts Chem. Res.* **2010**, *43*, 1080.

[20] a) D. H. M. Dam, K. S. B. Culver, I. Kandela, R. C. Lee, K. Chandra, H. Lee, C. Mantis, A. Ugolkov, A. P. Mazar, T. W. Odom, *Nanomedicine* **2015**, *11*, 671; b) D. H. M. Dam, J. H. Lee, P. N. Sisco, D. T. Co, M. Zhang, M. R. Wasielewski, T. W. Odom, *ACS Nano* **2012**, *6*, 3318; c) K. Chandra, K. S. B. Culver, S. E. Werner, R. C. Lee, T. W. Odom, *Chem. Mater.* **2016**, *28*, 6763.

[21] E. A. Appel, M. W. Tibbitt, M. J. Webber, B. A. Mattix, O. Veiseh, R. Langer, *Nat. Commun.* **2015**, *6*, 6295.

[22] a) L. W. Xia, R. Xie, X. J. Ju, W. Wang, Q. M. Chen, L. Y. Chu, *Nat. Commun.* **2013**, *4*; 2226; b) S. H. Jiang, F. Y. Liu, A. Lerch, L. Ionov, S. Agarwal, *Adv. Mater.* **2015**, *27*, 4865.

[23] Y. Q. Li, B. W. Zhu, Y. G. Li, W. R. Leow, R. Goh, B. Ma, E. Fong, M. Tang, X. D. Chen, *Angew. Chem. Int. Edit.* **2014**, *53*, 5837.

[24] S. A. Ranamukhaarachchi, S. Lehnert, S. L. Ranamukhaarachchi, L. Sprenger, T. Schneider, I. Mansoor, K. Rai, U. O. Häfeli, B. Stoeber, *Sci. Rep.* **2016**, *6*, 32074.

[25] M. C. Giano, Z. Ibrahim, S. H. Medina, K. A. Sarhane, J. M. Christensen, Y. Yamada, G. Brandacher, J. P. Schneider, *Nat. Commun.* **2014**, *5,* 4095.

[26] a) N. S. Dhillon, J. Buongiorno, K. K. Varanasi, *Nat. Commun.* **2015**, *6*; 8247; b) D. I. Yu, H. J. Kwak, H. Noh, H. S. Park, K. Fezzaa, M. H. Kim, *Sci. Adv.* **2018**, *4*. e1701571.

[27] J. Zhuang, C. Q. Huang, G. Zhou, Z. M. Liu, H. Xu, D. M. Wu, Y. Q. Fan, Y. J. Zhang, *Appl. Therm. Eng.* **2016**, *102*, 1473.

[28] a) F. Wang, W. W. Gao, S. Thamphiwatana, B. T. Luk, P. Angsantikul, Q. Z. Zhang, C. M. J. Hu, R. H. Fang, J. A. Copp, D. Pornpattananangkul, W. Y. Lu, L. F. Zhang, *Adv. Mater.* **2015**, *27*, 3437; b) G. Han, L. R. Martinez, M. R. Mihu, A. J. Friedman, J. M. Friedman, J. D. Nosanchuk, *Plos One* **2009**, *4*, e7804.

[29] R. Prabhakara, O. Foreman, R. De Pascalis, G. M. Lee, R. D. Plaut, S. Y. Kim, S. Stibitz, K. L. Elkins, T. J. Merkel, *Infect. Immun.* **2013**, *81*, 1306.

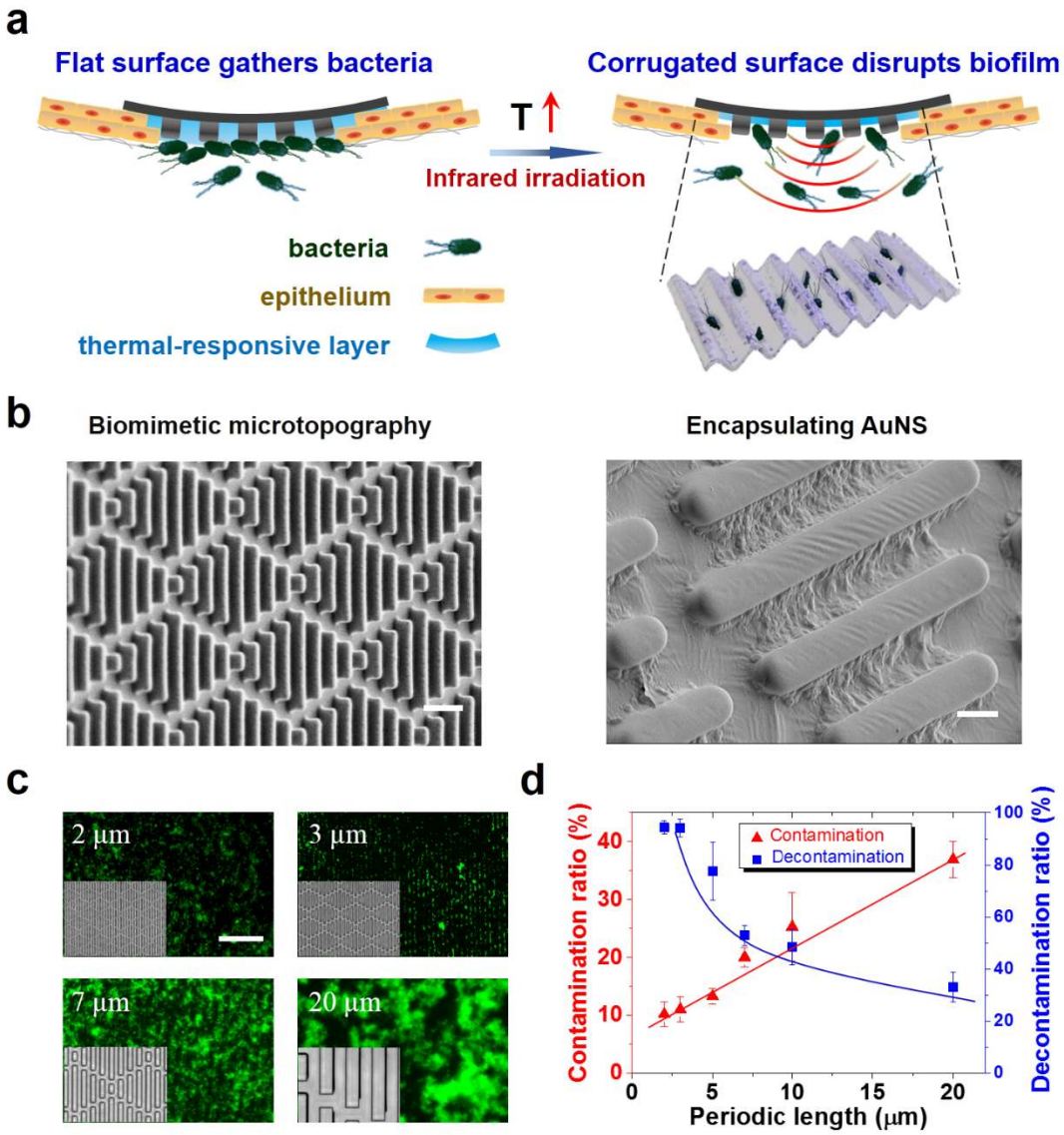

Figure 1 Design features and proposed mechanism of TRIM integrating biomimetic topography to reduce aggregation of attached bacteria and prevent the formation of biofilm. **(a)** Thermal-disrupting film exhibits flat surface normally while reproducing corrugated microtopography during heating (*via* infrared-light irradiation). The corrugated surface would induce thermally activated disruption of the biofilm and facilitate the ablation of planktonic bacteria, while mitigating the thermal harm to host epithelium. **(b)** PDMS film with topography mimicking the feature of shark-skin before (left) and after (right) integration with AuNS. Scale bars: 10 μm (left) and 3 μm (right). **(c)** Fluorescence images show that *S. aureus* (green) attached within feature gaps when dispersed on films with 2-μm and 3-μm features. On surfaces with 5-μm and larger features, *S. aureus* formed aggregates. Inset in **c** are from one measurement representative of contamination experiments. Scale bar: 50 μm. **(d)** Graph shows films with larger periodic length of surface feature enhance bacterial growth and biofilm formation (red curve). Bacteria within biofilms are more difficult to decontaminate (blue curve). Error bars are obtained from 7 measurements for each point (N=7).

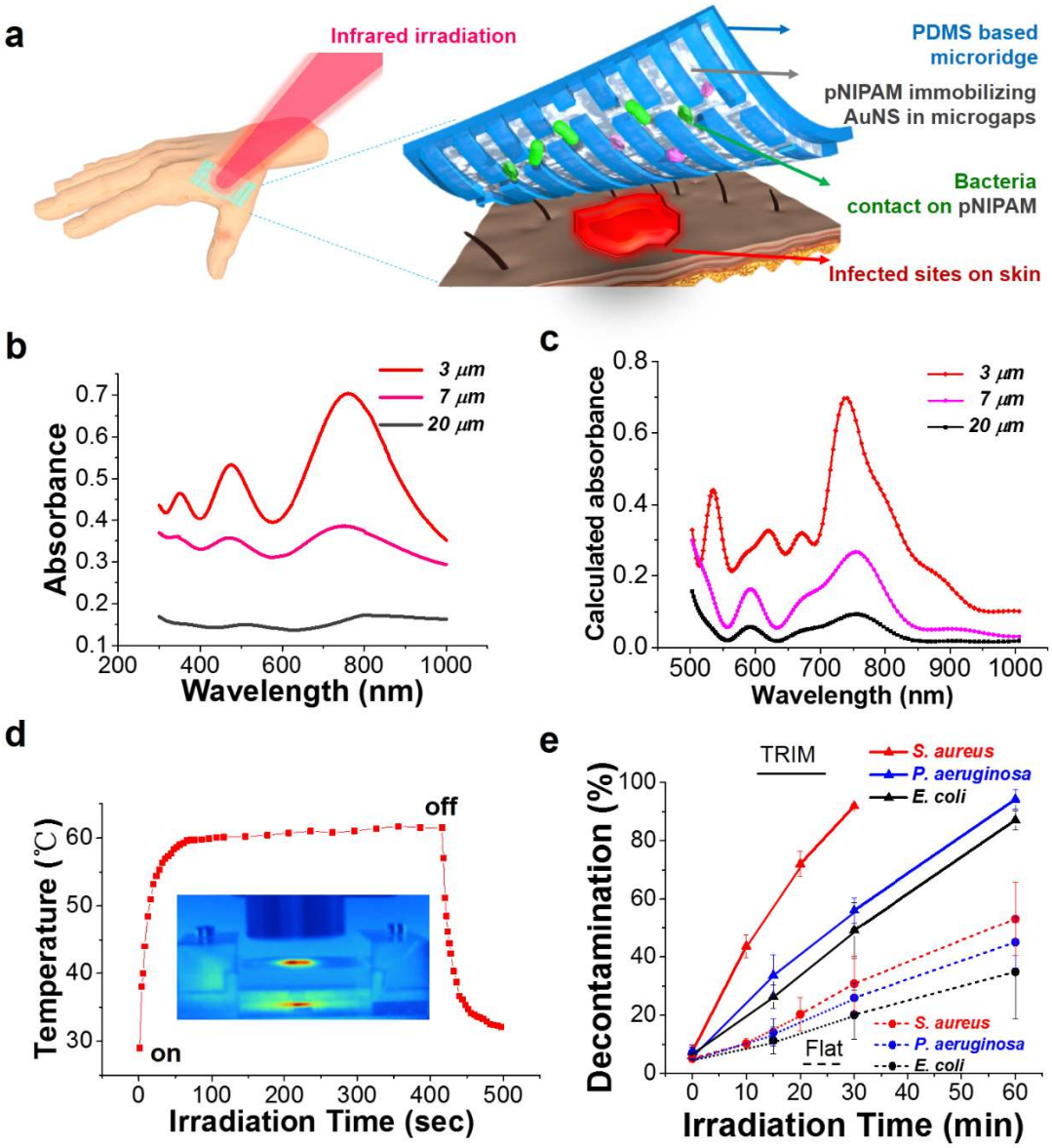

Figure 2 ***In vitro*** **assessment of the TRIM films for photothermal elimination of various bacteria. (a)** Illustration shows a TRIM film attached on the skin absorbs infrared light and generates local heat, which kills bacteria in the depressed regions of the film while leaving the surrounding epithelial host cells unharmed. **(b)** UV-visible absorption spectra show that films with smaller features had higher absorbance. **(c)** FDTD simulations confirm that microstructures have enhanced absorbance. **(d)** Graph shows the surface temperature of a TRIM film (integrated with AuNS of concentration of 0.2 nM) is maintained below 60 °C during NIR irradiation (70 mW/cm^2) and rapidly decreases when irradiation is turned off. Inset: infrared camera image. **(e)** Survival curves of gram-negative bacterium, *E. coli*, *P. aeruginosa* and gram-positive bacterium, *S. aureus* on either the TRIM films or flat films. TRIM films with microstructured topography that disrupt the formation of biofilms had better decontamination efficiency because bacteria on these surfaces were less tolerant to heat. Error bars are obtained from 7 measurements for each point (N=7).

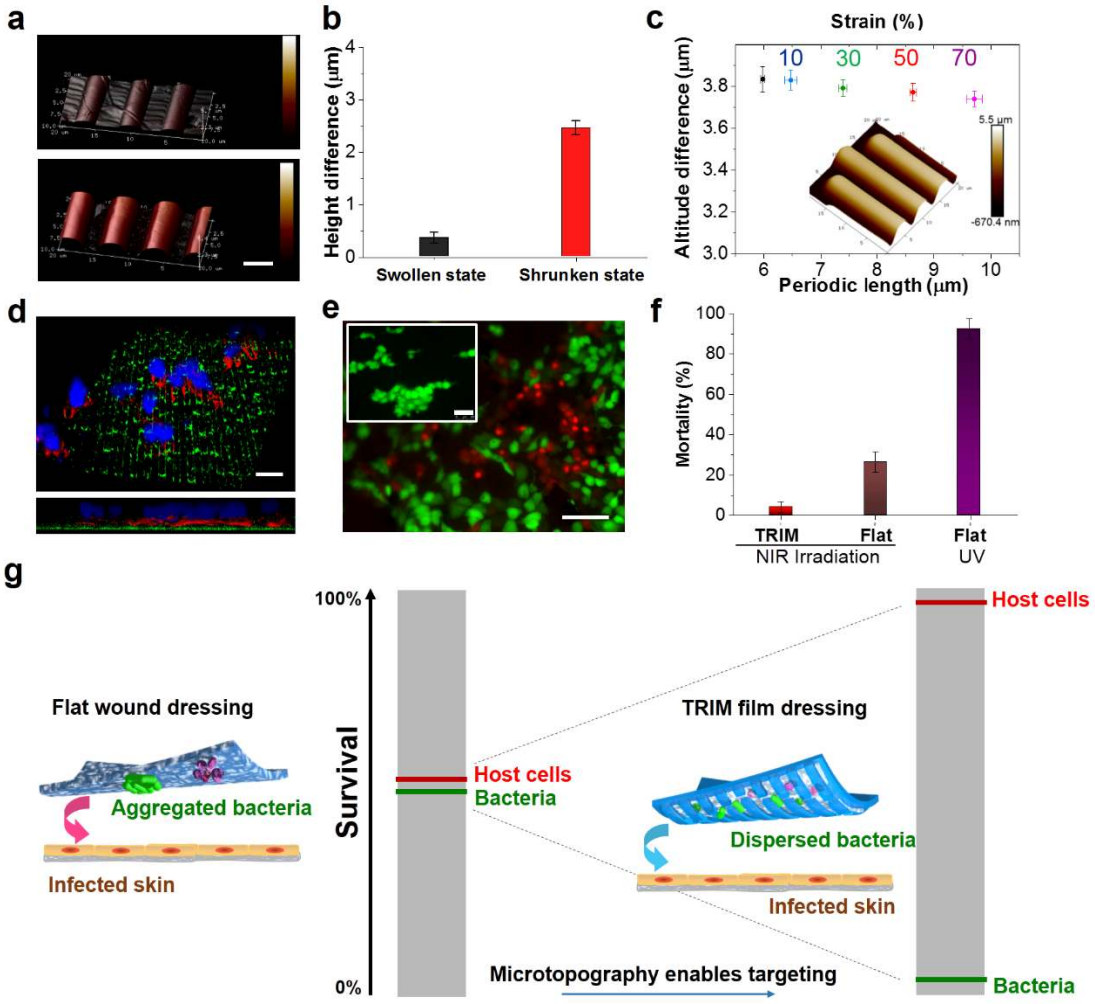

Figure 3 TRIM films as antibacterial dressings. (a) AFM image of TRIM films at 25 °C (top) and 42 °C (bottom). pNIPAM shrinks and wraps the surface features at temperatures above its LCST of 32 °C. Scale bars: 5 μm. **(b)** Height difference between microridge and depressed regions on the TRIM films as measured by AFM at temperatures below (swollen state) and above (shrunken state) the LCST of pNIPAM (error bars: N=7). **(c)** Height difference between microridge and depressed regions was maintained after stretching the films to 70% (error bars: N=7). Inset shows AFM image of the film before stretch. **(d)** Confocal fluorescence microscope images at top view (top) and sectional view (bottom) show MDCK cells are suspended above the depressed regions. Surface features are labeled with FITC-conjugated nanoparticles (green), cell nucleus is stained with DAPI (blue) and the cytoskeleton (F-actin) is stained with phalloidin (red). Scale bar: 20 μm. **(e)** Fluorescence images of MDCK cells on TRIM films (inset) and flat films under NIR irradiation (70 mW/cm^2) show that nearly all cells on TRIM films survived after irradiation. Cells are co-stained with calcein AM and propidium iodide to differentiate live cells (green) from dead cells (red). Scale bars: 50 μm. **(f)** Mortality assay show MDCK cells survived better on biomimetic surfaces than flat surfaces upon NIR irradiation. UV irradiated flat surface was positive control. **(g)** Illustration showing that the survival dichotomy of bacteria and host cells during phototherapy is induced by the biomimetic topography-decorated wound dressing.

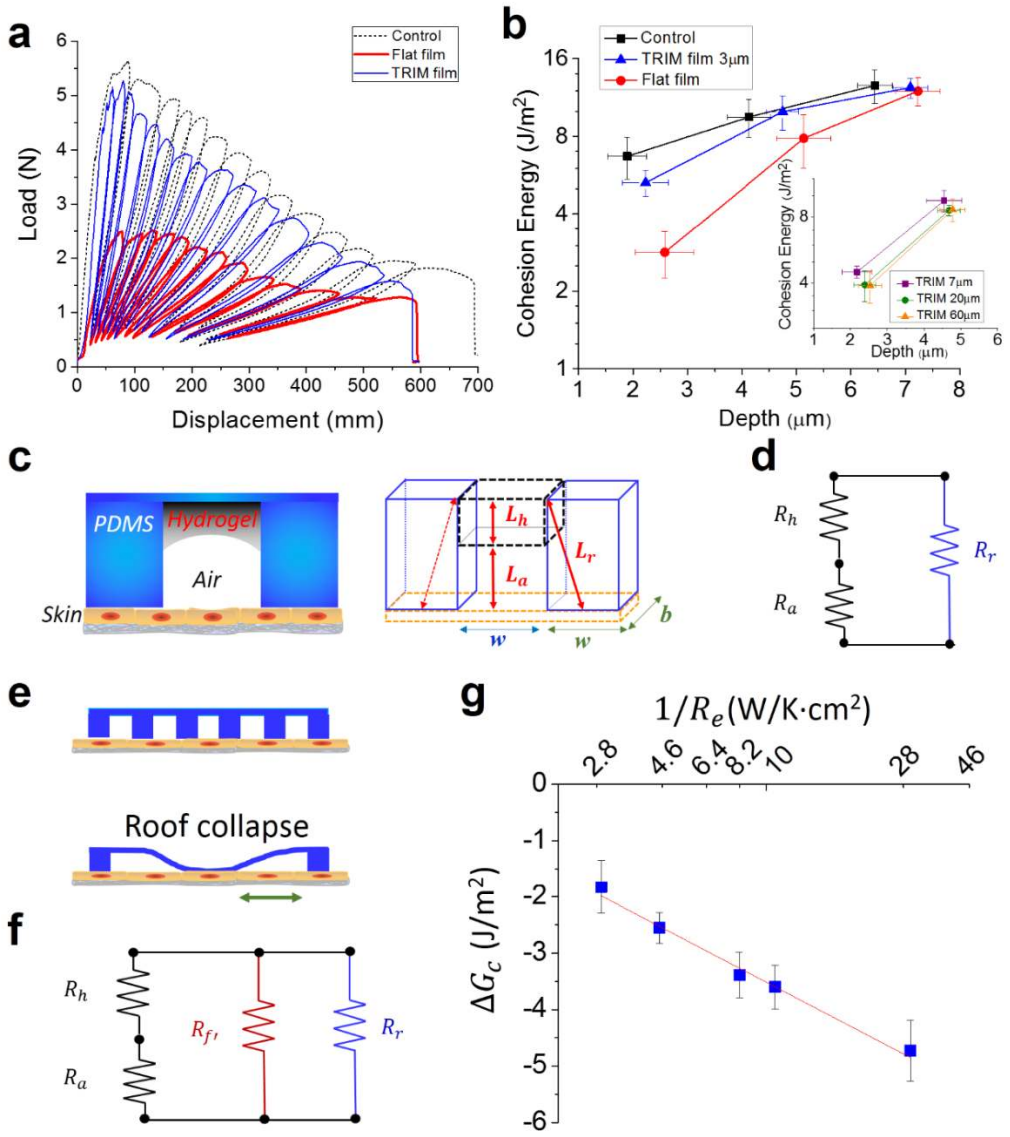

Figure 4 Microstructures on the TRIM films reduce photothermal-induced loss in intercellular cohesion of human epidermis. (a) Critical load as a function of displacement (distance between the two DCB substrate during delamination test) for native SC (control, grey), SC after treatment by irradiation with flat film (red) and TRIM film with 3-μm feature size (blue) in delamination tests. SC detached most easily after irradiation treatment by flat films. **(b)** Cohesion energy as a function of depth of SC tissue attached onto various substrates. Films with large surface features led to greater loss in intercellular cohesion. Error bars are obtained from 12 measurements for each point (N=12). **(c)** Schematic of the biointerface between the photothermal film and skin tissue (left), and dimensional profile of each component for thermal conduction (right). **(d)** Illustration of the compound thermal resistance for an unsagged TRIM film. **(e)** Schematic diagram of a hydrogel roof collapse occurring between skin and film when the width to depth ratio of the microvalley is greater than the critical width of 20 μm and critical depth of 60 μm. **(f)** Illustration of the compound thermal resistance for a TRIM film experiencing a hydrogel roof collapse. **(g)** Cohesion energy loss as a function of compound thermal resistances. Error bars are obtained from 12 measurements for each point (N=12).

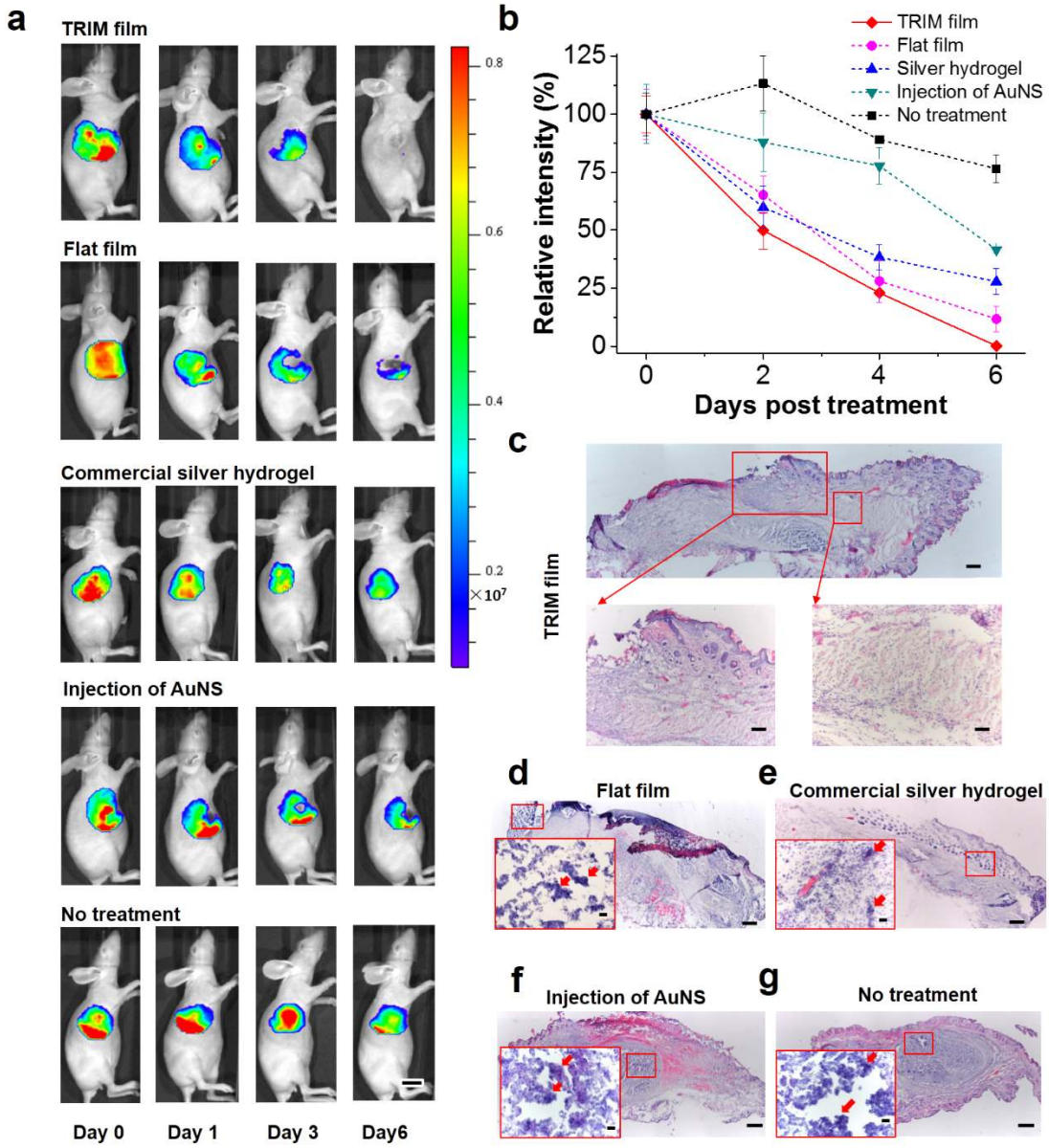

Figure 5 ***In vivo*** **assessment of different treatments on the** ***S. aureus*** **infected mice. (a)** Fluorescence images of mice at 1-, 3- and 6-days post-treatment. (group 1 to 5) show that TRIM films had the best healing performance. Scale bar: 1 cm. **(b)** Quantification of the total radiant efficiency (normalized to the initial radiant efficiency at day 0) as observed in (a), N=6 for statistic studys. **(c-g)** Hematoxylin/Eosin (H&E) staining of tissues from the infected sites reveal that TRIM film is most effective (**c**). Scale bars: upper, 200 µm; lower left, 100 µm; lower right, 50 µm. Obvious inflammatory reactions were seen in **(d-g)** All scale bars: 200 µm; scale bars in inset: 50 µm.

The table of contents entry

A localized thermal managing strategy from thermal-disrupting interface induced mitigation (TRIM) is developed to maintain intercellular cohesion and reduce function loss of epidermis tissue for topical antibacterial therapy. The dressing film with TRIM effect inhibit aggregation of bacteria, promote selective elimination of pathogens, and shortens the healing process.

Thermal-disrupting interface mitigates intercellular cohesion loss for accurate topical antibacterial therapy

Benhui Hu, Christopher Berkey, Timothy Feliciano, Xiaohong Chen, Zhuyun Li, Chao Chen, Shahrouz Amini, Mui Hoon Nai, Qun-Li Lei, Ran Ni, Juan Wang, Wan Ru Leow, Shaowu Pan, Yong-Qiang Li, Pingqiang Cai, Ali Miserez, Shuzhou Li, Chwee Teck Lim, Yun-Long Wu,* Teri W. Odom,* Reinhold H. Dauskardt* and Xiaodong Chen**